Vertical Structure of Convective Heating and the Three-Dimensional Structure of the Forced Circulation on an Equatorial Beta Plane*

ZHAOHUA WU, E. S. SARACHIK, AND DAVID S. BATTISTI

Department of Atmospheric Sciences, University of Washington, Seattle, Washington

(Manuscript received 24 August 1998, in final form 21 July 1999)

ABSTRACT

In this paper, the three-dimensional structure of the thermally forced atmosphere on an equatorial β plane is investigated. Special emphasis is placed on the relations between the vertical structure of heating and the horizontal structure of the forced response.

By solving the vertical eigenvalue–eigenfunction problem in a vertically semi-infinite domain, the authors obtain a complete set of vertical eigenfunctions that includes a single barotropic (external) mode and a continuous spectrum of baroclinic (internal) modes. These eigenfunctions are used to decompose vertical heating profiles for two types of tropical heating: 1) deep heating representing the convective plume (CP) heating and 2) shallow heating representing mature cloud (MC) cluster heating. By examining the spectral energy density of the heating profile, the contributions of each vertical mode (spectral interval) to the overall structure are explored for each case, and the difference between the responses to these two profiles of heating is discussed. A dry spectral primitive equation model of the atmosphere is employed to verify the analytical results.

The results from both the analytical approach and the numerical simulations are consistent in showing that the vertical structure of the heating is fundamental to the structure of the forced response. The CP is deep relative to the MC. Thus, the CP projects onto the vertical eigenfunctions of relatively larger equivalent depth more so than does the MC. As a result, the CP-forced signals propagate away from the heat source much faster than those forced by the MC. Hence, when the atmosphere is subjected to the same linear dampings (Rayleigh friction and Newtonain cooling), the spatial (mainly in the horizontal) decay rate of the CP-forced signals is significantly smaller than that of the MC-forced signals, and the CP-forced signals extend farther.

To what extent a shallow-water system of a specified vertical mode (e.g., the Gill model) can approximate the three-dimensional response is also examined. Results show that the effective gravity wave speed of the multimode system varies greatly with location. Hence, it is extremely difficult to select a globally suitable equivalent depth so that a one-mode shallow-water system can approximate the spatially three-dimensional structure of the response to a given heating.

1. Introduction

The most notable precipitation features are the organized high rainfall regions in equatorial latitudes that are associated with strong convection (e.g., Peixoto and Oort 1992). Especially noteworthy are the very high values of precipitation over the equatorial regions in South America, Africa, Indonesia, and in the equatorial Pacific Ocean, implying substantial thermal forcing of the atmosphere in these regions.

The significant influence of the variations in tropical thermal sources on the tropical and extratropical circulations has been recognized and explored through many observational and modeling studies. Among these studies, Horel and Wallace (1981) demonstrated that the Northern Hemisphere geopotential height fields in wintertime exhibit well-defined teleconnections with the tropical heating. Simmons (1982), using a linear primitive equation model, simulated the global circulations driven by a steady tropical heat source and showed that the modeled circulations agreed well with the observations. Moura and Shukla (1981) suggested that the drought over northeast Brazil might be due to the intensification of the intertropical convergence zone (ITCZ), located to the north of the equator, which occurs in association with warm sea surface temperature (SST) anomalies, and the establishment of descending motion over northeast Brazil and cold water anomalies in the subtropical southern Atlantic, which reduces moist convection and rainfall. Rodwell and Hoskins (1996), by modeling the zonal overturning driven by monsoon heating in the Indian subcontinent, emphasized the role of thermal sources in the formation of subtropical deserts such as the Sahara.

* Joint Institute for the Study of the Atmosphere and Ocean Contribution Number 587.

Corresponding author address: Zhaohua Wu, COLA, 4041 Powder Mill Rd., Suite 302, Calverton, MD 20705.
E-mail: wu@cola.iges.org

Parallel to these observational and modeling studies, theoretical advances were also made to account for the response of the tropical atmosphere to thermal forcing. These efforts involved solving a set of linear equations on an equatorial β plane that governs the spatially three-dimensional tropical atmosphere. These efforts can be crudely classified into two categories: 1) the tidal approach and 2) the shallow-water approach.

In the tidal approach, after assuming the time periodicity of the solution and using the Fourier transform in the zonally cyclic domain, one can separate the equation for the mass-weighted meridional velocity into a nonhomogeneous vertical structure equation and a homogeneous meridional structure equation. By solving the homogeneous meridional structure equation with appropriate boundary conditions at the infinities, one obtains the separation constants (which are the eigenvalues, historically called ''the equivalent depths'' in this context) and their corresponding meridional eigenfunctions. With a known separation constant, the nonhomogeneous vertical structure equation is solved to obtain the vertical structure of the forced response for each meridional mode. The details of this approach can be found in the classic paper of Lindzen (1967). Lindzen (1968) further used this approach to explore the forced waves in the presence of Newtonian cooling. Dickinson and Geller (1968) showed that this approach can be extended to the case in which the thermal damping has more complicated vertical structure.

A bothersome problem associated with the tidal approach is the completeness of the meridional eigenfunctions on a meridionally infinite equatorial β plane. The completeness of these meridional eigenfunctions has long been assumed (Lindzen 1967) and can be shown (Wu 1998; Wu et al. 1999) using a method similar to that of Holl (1970), who showed the completeness of the Hough functions. However, the eigenvalues and the corresponding eigenfunctions were not fully discovered until recently (D. Moore 1997, personal communications; see also Wu 1998). The complete set of eigenfunctions on a meridionally infinite equatorial β plane includes three types: 1) the eigenfunctions of discrete positive eigenvalue, which shrink to the equator as frequency goes to zero; 2) the eigenfunctions of discrete positive eigenvalue, which approach either of two sinusoidal functions (with one symmetric and the other antisymmetric about the equator) before they reach their turning points; and 3) the eigenfunctions of continuous negative eigenvalue. The first two types of eigenfunctions were discussed in Lindzen (1967), Lindzen and Matsuno (1968), Philander (1990), and Wu et al. (1999). The third type of eigenfunction was recently discovered by Moore and discussed in detail in Wu (1998) and Wu et al. (1999). Wu et al. (1999) also showed that a prescribed large-scale, low-frequency heat source mainly projects onto the eigenfunctions of continuous negative eigenvalue. However, methods still need to be developed to calculate the projection of the forcing onto these eigenfunctions.

The tidal approach has been quite successful in studying diurnal tides (Lindzen 1967), but it has not been widely used to understand the forced response to a large-scale, low-frequency heat source for two reasons. First, many investigators have not recognized that a continuous spectrum of eigenfunctions of negative eigenvalue, in addition to the discrete eigenfunctions of positive eigenvalue, is defined by the meridional eigenvalue–eigenfunction problem. Instead, they believed that the eigenfunctions defined by the meridional eigenvalue–eigenfunction problem on an equatorial β plane did not form a complete set, and hence, the variable separation method could not be used because the tidal approach would not provide an appropriate description of the atmospheric (and oceanic) response to given types of tropical heating. They regarded this as one of the flaws of a infinite equatorial β plane. Second, at low frequencies, momentum damping can not be neglected. To obtain a nonhomogeneous vertical structure equation and a homogeneous meridional structure equation, one must first perform a Fourier transform in the zonal direction. In the presence of momentum damping, however, this means that the mass-weighted meridional velocity equation separates into a nonhomogeneous vertical structure equation and a homogeneous meridional structure equation that has complex coefficients. For such a meridional structure equation, the completeness of the eigenfunctions is not guaranteed. Hence, using the variable separation method in the presence of momentum damping is again questionable.

Although the first problem associated with the tidal approach has been dealt with in Wu et al. (1999), confirming the completeness of the eigenfunctions defined by the meridional eigenvalue–eigenfunction problem, the second problem is not solved. Thus, the tidal approach is not clearly capable of studying the forced large-scale, low-frequency viscous response in the tropical atmosphere, and alternative approaches must be found. The shallow-water approach has been one of the most popular alternative approaches.

In the shallow-water approach, one separates the solution into a height-dependent part and a part that depends on the horizontal coordinates and time. The height-dependent part of the solution is expressed in terms of the vertical eigenfunctions (the vertical modes), which are obtained through the solution of the vertical structure equation under appropriate boundary conditions. For each of these vertical modes, variations of the solution in a horizontal position and time are governed by the forced shallow-water equations but with a different equivalent depth of water for each vertical mode. The overall solution is the summation of the contributions from each vertical mode.

The inviscid linear shallow-water system on an equatorial β plane was first solved by Matsuno (1966) in his study of free and forced waves in the Tropics. Since

then, many studies have used the shallow-water system with a prescribed equivalent depth and linear damping (usually Rayleigh friction and Newtonian cooling) to describe the low-frequency responses in both the Tropics and extratropics to tropical thermal sources. Among them, Lau and Lim (1982) discussed the Hadley and Walker circulations associated with the east Asian winter monsoon, Lim and Chang (1983) focused on the dynamics of teleconnections and the Walker circulations forced by equatorial heating, and Zhang and Krishnamurti (1996) calculated the circulations driven by the global tropical thermal sources and sinks, which are inferred from a satellite-based field of the outgoing longwave radiation.

The most influential, albeit simple, study using such an approach is the Gill (1980) model. In his model, Gill assumed that the important contributions to the solution come only from modes with inverse vertical wavenumbers that are of the same order as the scale of the forcing function. In his paper, he selected only one vertical mode, which was an idealized heat source that had the structure of a single sinusoid from the surface to the tropopause with maximum heating in the midtroposphere, to illustrate the horizontal structure of the response of the tropical atmosphere to a thermal source. To obtain this normal mode representation, Gill implicitly imposed a lid at the top of the heating. Hence, the vertical structure of the solution is the same as the vertical structure of a vertically standing free mode that is generated by the artificial lid (Lindzen et al. 1968). The solutions to his model are essentially similar to the circulations simulated by Webster (1972) using a two-layer numerical model.

Although Gill's solution is sometimes recognized as a good approximation of the horizontal structure of the response to an isolated large-scale thermal source in the Tropics, there are several problems associated with this model. One problem is that the heating is artificially brought down to the surface whereas the actual heating due to release of latent heat of condensation occurs above the cloud base. Hence, the vertical transfer of heating from the cloud base to the surface, which is extremely important in understanding the thermally forced surface winds in the Tropics, cannot be explored. To overcome this drawback, Geisler and Stevens (1982) introduced the multimode method by imposing a rigid lid somewhere above the top of the heating and used the sum of all the (discrete) vertical normal modes to cancel the artificial heating induced by the Gill model outside of the heating layers. Similar multimode methods were widely used later (e.g., Silva Dias et al. 1983; Kasahara 1984; DeMaria 1985; Mapes and Houze 1995; Mizzi et al. 1995). Silva Dias (1986) also examined the sensitivity of the vertical mode expansion to the location of the upper boundary of the model atmosphere and to the vertical resolution.

Although the multimode method improves the overall solution, this method also has drawbacks. The real atmosphere is semi-infinite in the vertical, and the extent of the effects that the imposed lid has on the response requires further investigation. Machenhauer and Daley (1974) and Eliassen and Machenhauer (1974) showed that changing the upper-boundary condition not only affects the model results but also affects the computational stability associated with the model integration. Mapes and Houze (1995) demonstrated that the truncation of the vertical modes greatly affects the amplitude of the simulated surface winds. DeMaria (1985) and Mizzi et al. (1995) used similar vertical structure equations with corresponding lids at different heights to define the vertical eigenfunctions. Their results showed that the structure of the eigenfunctions are sensitively dependent on the height of the lid and that to diminish the effect of the lid, many vertical modes must be retained to obtain an accurate solution.

It should be noted that in both the tidal approach and the shallow-water approach, the separation constant (eigenvalue) has historically been called the equivalent depth. However, the meaning of the separation is different in these two different approaches. Mathematically, the separation constant is uniquely determined by the eigenvalue–eigenfunction problem. Since the eigenvalue–eigenfunction problems are different in the tidal approach and in the shallow-water approach, it is anticipated that the resulting sets of separation constants are different. Physically, most of the positive eigenvalue modes in the tidal approach represent the vertically propagating waves, and all the negative eigenvalue modes represent vertically trapped solutions (Philander 1990). However, in the shallow-water approach, a positive eigenvalue of a vertical mode represents the depth of a hypothetical homogeneous fluid, which describes the horizontal structure of the horizontal velocities and the geopotential perturbation of that particular vertical mode. Hence, only in the shallow-water approach can the equivalent depth (the separation constant) represent the depth of a homogeneous fluid; the equivalent depth (the separation constant) in the tidal approach is only a mathematical symbol for the eigenvalue that only looks like the equivalent depth.

In this paper, we will develop a vertical decomposition method that is free of the previously mentioned drawbacks in order to investigate the thermally forced tropical atmosphere. Geisler (1981) and Hartmann et al. (1984) showed that the vertical structure of the thermally forced response is significantly affected by the vertical structure of the heating. Lau and Peng (1987) and Sui and Lau (1989) showed that zonal propagation speed of the forced signal is sensitive to the vertical structure of the prescribed heating. However, a complete theoretical argument to explain why and how such relations exist has not yet been given. By calculating the projections of a prescribed vertical heating profile onto the vertical eigenfunctions, we will examine the contribution of different modes to the overall solution and then further clarify how the vertical structure of heating

affects the three-dimensional (especially horizontal) structure of the response. In section 2, we separate the linear equations into a vertical structure equation and a set of shallow-water equations. In section 3, we solve the vertical eigenvalue–eigenfunction problem in a semi-infinite atmosphere with a radiation condition at the top of the atmosphere. We project two thermal sources onto the vertical eigenfunctions in section 4 and discuss how the horizontal structure of the response to the convective plume (CP) heating is different from that of the response to the mature cloud (MC) cluster heating. To verify the analytical results, we also carry out a series of numerical experiments in a dry primitive equation general circulation model in section 5. The summary and conclusions are presented in section 6.

2. Basic equations

The linear equations in log pressure coordinates for the tropical atmosphere on an equatorial β plane are

$$\left(\frac{\partial}{\partial t} + \alpha\right)u^* - \beta y v^* = -\frac{\partial \Phi^*}{\partial x}, \quad (2.1a)$$

$$\left(\frac{\partial}{\partial t} + \alpha\right)v^* + \beta y u^* = -\frac{\partial \Phi^*}{\partial y}, \quad (2.1b)$$

$$\frac{\partial u^*}{\partial x} + \frac{\partial v^*}{\partial y} + \frac{1}{\rho_0}\frac{\partial(\rho_0 w^*)}{\partial z^*} = 0, \quad \text{and} \quad (2.1c)$$

$$\left(\frac{\partial}{\partial t} + \gamma\right)\left(\frac{\partial \Phi^*}{\partial z^*}\right) + N^2 w^* = \frac{\kappa J}{H}, \quad (2.1d)$$

where u^* (v^*) is the eastward (northward) velocity; w^* is the vertical velocity in log pressure coordinates; Φ^* is the geopotential; ρ_0 is the basic density; κ is the gas constant R divided by the heat capacity, c_p; J is the external heating rate per unit mass per unit time; N^2 is the buoyancy frequency squared; and H is a scale height. In $\beta = 2\Omega/a$, Ω and a are the earth's rotation rate and radius, respectively; α is Rayleigh friction coefficient; and γ is Newtonian cooling coefficient.

Equations (2.1) use an equatorial β plane approximation to the sphere and are standard for studying the tropical atmosphere (see, e.g., Holton 1992). Although the generalization to a nonisothermal atmosphere is straightforward, we simplify the algebra by assuming an isothermal atmosphere of temperature T_s. The basic state is taken to be motionless. Hence, the basic density ρ_0 satisfies

$$\rho_0(z^*) = \rho_0(0)e^{-z^*/H}. \quad (2.2)$$

To simplify Eqs. (2.1), we introduce the following mass-weighted variables: $u = \rho_0^{1/2}u^*$, $v = \rho_0^{1/2}v^*$, $w = \rho_0^{1/2}w^*$, and $\Phi = \rho_0^{1/2}\Phi^*$. These are substituted into Eqs. (2.1) using Eq. (2.2), and time dependence of the form $e^{-i\omega t}$ is assumed to obtain

$$(\alpha - i\omega)u - \beta y v = -\frac{\partial \Phi}{\partial x}, \quad (2.3a)$$

$$(\alpha - i\omega)v + \beta y u = -\frac{\partial \Phi}{\partial y}, \quad (2.3b)$$

$$\frac{\partial u}{\partial x} + \frac{\partial v}{\partial y} + \left(\frac{\partial}{\partial z} - \frac{1}{2H}\right)w = 0, \quad \text{and} \quad (2.3c)$$

$$(\gamma - i\omega)\left(\frac{\partial}{\partial z} + \frac{1}{2H}\right)\Phi + wN^2 = Q, \quad (2.3d)$$

where the superscript "*" has been omitted and $Q = \rho_0^{1/2}\kappa J/H$.

Eliminating w from Eqs. (2.3c) and (2.3d) leads to

$$\frac{\gamma - i\omega}{N^2}\left(\frac{\partial^2}{\partial z^2} - \frac{1}{4H^2}\right)\Phi - \left(\frac{\partial u}{\partial x} + \frac{\partial v}{\partial y}\right) = \left(\frac{\partial}{\partial z} - \frac{1}{2H}\right)\frac{Q}{N^2}. \quad (2.4)$$

The vertical eigenfunctions are defined by the equation

$$\frac{d^2V_m}{dz^2} + \left(\frac{N^2}{gh_m} - \frac{1}{4H^2}\right)V_m = 0, \quad (2.5)$$

and the boundary conditions are defined as

$$\frac{dV_m}{dz} + \frac{V_m}{2H} = 0, \text{ at } z = 0, \quad \text{and} \quad (2.6a)$$

either $V_m \to 0$ *or outgoing radiation condition,* as $z \to \infty$. (2.6b)

Equation (2.5) and its boundary conditions [Eqs. (2.6a) and (2.6b)] define a complete set of eigenfunctions in the vertical under the concept of analytical continuation[1] (details are found in the sections about the continuous spectrum in chapter 4 of Friedman 1956).

By expanding the variables in Eqs. (2.3a), (2.3b), and (2.4) in terms of the vertical eigenfunctions V_m, that is,

[1] Since Eq. (2.5) is defined in an infinite domain, a relatively small positive equivalent depth renders a solution that is not Lebesgue square integrable in an interval containing infinity. In such a case, the differential operator in Eq. (2.5) is said to be in the *limit-point* case at infinity. The principle of analytic continuation requires that in such a case, the corresponding Green's function is defined by implicitly requiring the Green's function to vanish for large values of z if $\lambda = (N^2/gh_m - 1/4H^2)$ is complex and $\mathrm{Im}\sqrt{\lambda} > 0$. For real values of λ, the Green's function is defined as the limit of the Green's function for complex values of λ as λ approaches the real axis. Hence, the differential operator in an infinite domain with a radiation boundary condition can be treated in the same way as when it is defined in a finite domain with regular (e.g., homogeneous, linear, incoming waves, outgoing waves, etc.) boundary conditions.

$$\begin{bmatrix} u \\ v \\ \Phi \end{bmatrix} = \sum_m \begin{bmatrix} u_m(x, y) \\ v_m(x, y) \\ \Phi_m(x, y) \end{bmatrix} V_m(z), \tag{2.7}$$

one obtains

$$(\alpha - i\omega)u_m - \beta y v_m = -\frac{\partial \Phi_m}{\partial x}, \tag{2.8a}$$

$$(\alpha - i\omega)v_m + \beta y u_m = -\frac{\partial \Phi_m}{\partial y}, \quad \text{and} \tag{2.8b}$$

$$\frac{(\gamma - i\omega)}{gh_m}\Phi_m + \left(\frac{\partial u_m}{\partial x} + \frac{\partial v_m}{\partial y}\right) = -F_m, \tag{2.8c}$$

where F_m satisfies

$$\tilde{Q} = \left(\frac{\partial}{\partial z} - \frac{1}{2H}\right)\frac{Q}{N^2} = \frac{\kappa}{N^2 H}\left(\frac{\partial}{\partial z} - \frac{1}{2H}\right)(\rho_0^{1/2} J) = \sum_m F_m(x, y)V_m(z) \tag{2.9}$$

and the summation represents a sum over the discrete spectrum and an integration over the continuum.

3. The vertical eigenvalue–eigenfunction problem

We rewrite Eq. (2.5) as

$$\frac{d^2 V_m}{dz^2} + \lambda_m V_m = 0, \tag{3.1}$$

where

$$\lambda_m = \left(\frac{N^2}{gh_m} - \frac{1}{4H^2}\right). \tag{3.2}$$

The boundary conditions are given by Eqs. (2.6a) and (2.6b).

As described in Holton (1975), the eigenfunctions defined by Eq. (3.1) and its boundary conditions include a continuous spectrum of modes that vary sinusoidally with height and one additional mode (the Lamb mode) for which the vertical displacement is zero but the pressure perturbation decays exponentially with height. Holton (1975) did not give the explicit expressions of these eigenfunctions. To obtain these eigenfunctions, we will use the method of the spectral representation of an differential operator; that is, we will construct the Green's function and integrate it around a large circle in the complex λ domain to represent a δ function. The details of the method can be found in Friedman (1956).

The Green's function $G(z, \xi, \lambda)$ is a solution of the equation

$$\frac{d^2 G}{dz^2} + \lambda G = -\delta(z - \xi), \tag{3.3}$$

which satisfies the lower boundary condition

$$G_z(0, \xi, \lambda) = -\frac{G(0, \xi, \lambda)}{2H}. \tag{3.4}$$

From (3.3), we see that

$$G = ae^{i\sqrt{\lambda}z} + be^{-i\sqrt{\lambda}z} \quad \text{for } z \neq \xi. \tag{3.5}$$

If λ is complex or if λ is real and negative, one of the terms on the right-hand side in this expression goes exponentially to infinity and the other goes exponentially to zero as $z \to \infty$. It is clear then that for these values of λ, the Green's function is Lebesgue integrable if, and only if, it goes to zero exponentially for large values of z. For real positive values of λ, both terms are bounded at infinity, and neither the term, nor the linear combination, is Lebesgue integrable. We therefore apply the principle of analytic continuation and define the Green's function for real positive values of λ to be the limit of the Green's function with complex λ as λ approaches the real axis.

This definition still does not specify the Green's function uniquely because λ may approach the positive real axis from above or from below, and these two different approaches give different Green's functions. If we consider values of λ such that $\text{Im}\sqrt{\lambda} > 0$, the Green's function for real positive values of λ behaves like a multiple of $e^{i\sqrt{\lambda}z}$ for large values of z. On the other hand, if we consider values of λ such that $\text{Im}\sqrt{\lambda} < 0$, the Green's function for real positive values of λ behaves like a multiple of $e^{-i\sqrt{\lambda}z}$ for large values of z. Since we have already assumed a time factor $e^{-i\omega t}$, only the Green's function defined by analytic continuation from the Green's function for $\text{Im}\sqrt{\lambda} > 0$ behaves like "outgoing waves" for large values of z. Henceforth, the "Green's function" refers to the Green's function that represents outgoing waves at infinity and automatically satisfies "the radiation boundary" at infinity. From the description above, "the radiation condition" is both physically and mathematically the natural boundary condition for a vertically semi-infinite atmosphere.

Let us now return to the solutions of (3.3) and (3.4) for complex values of λ. We assume that $0 < \arg\lambda < 2\pi$ and choose the branch of the square root for which

$$0 < \arg\sqrt{\lambda} < \pi. \tag{3.6}$$

The term $e^{i\sqrt{\lambda}z}$ vanishes exponentially as z approaches infinity. Consequently, one determines coefficients a and b in Eq. (3.5) by using the continuous requirement and derivative jump requirement:

$$\left.\frac{dG}{dz}\right|_{\xi^-}^{\xi^+} = -1, \tag{3.7}$$

for G at $z = \xi$. The solution for G is

$$G = \left(\cos\sqrt{\lambda}z - \frac{1}{2H\sqrt{\lambda}}\sin\sqrt{\lambda}z\right) \times \frac{e^{i\sqrt{\lambda}\xi}}{i\sqrt{\lambda} + 1/(2H)}\mathcal{H}(\xi - z) + \left(\cos\sqrt{\lambda}\xi - \frac{1}{2H\sqrt{\lambda}}\sin\sqrt{\lambda}\xi\right) \times \frac{e^{i\sqrt{\lambda}z}}{i\sqrt{\lambda} + 1/(2H)}\mathcal{H}(z - \xi), \quad (3.8)$$

where $\mathcal{H}(\eta)$ is Heaviside unit function.

We obtain the expression of the $\delta(z - \xi)$ (details are in the appendix):

$$\delta(z - \xi) = \frac{1}{H}e^{-(z+\xi)/2H} + \frac{2}{\pi}\int_0^\infty \left(\cos mz - \frac{1}{2Hm}\sin mz\right) \times \left(\cos m\xi - \frac{1}{2Hm}\sin m\xi\right) \times \frac{m^2}{m^2 + 1/(4H^2)}\,dm. \quad (3.9)$$

Equation (3.9) states that the eigenfunctions defined by the vertical structure of Eq. (3.1) and its boundary conditions are complete and have two parts: a discrete mode that exponentially decays in the vertical and continuous modes of any vertical wavenumber. Hence, one obtains the discrete eigenfunction (often called the external mode or the barotropic mode) that has the form

$$V_e(z) = e^{-(z/2H)} \quad (3.10a)$$

and the continuous modes (often called the internal modes or the baroclinic modes) that have the form

$$V_{mi}(z) = \left(\cos mz - \frac{1}{2Hm}\sin mz\right)\frac{2Hm}{\sqrt{4H^2m^2 + 1}}, \quad (3.10b)$$

where m is any positive real number.

The discrete mode (3.10a) is often called the barotropic mode or external mode. Although the equivalent depth for this mode resulted from the vertical eigenvalue–eigenfunction problem approaching infinity, in the tidal approach (Lindzen 1967), this mode *is* the Lamb mode, which is regarded as a free mode with an equivalent depth of $H/(1 - \kappa)$. A feature of the Lamb mode is that the velocity everywhere is parallel to the earth's surface, that is, $w = 0$ (e.g., Gill 1982). The continuous modes represent all the baroclinic modes in a semi-infinite atmosphere. When the scale height H approaches infinity (the incompressible limit), the discrete mode disappears and the continuous modes become the Fourier integral in a semi-infinite domain.

This section shows that the shallow-water approach not only works for the vertically standing (free and forced) waves when an artificial lid is imposed but also is applicable to the vertically propagating forced waves. A key distinction between an atmosphere with a lid and a vertically semi-infinite atmosphere is that the free modes and the forced modes in the vertical are not distinguishable in an atmosphere with a lid; the zero vertical velocity requirement at the top and at the surface along with the vertical eigenvalue–eigenfunction equation defines the same complete set of vertical standing modes for both free and forced waves. For a vertically semi-infinite atmosphere, however, free vertically propagating baroclinic waves cannot survive since wave energy always radiates to space, leaving only the forced waves. These forced vertically propagating modes of wavelength $2\pi/m$ then have a horizontal structure of a shallow-water system of equivalent depth $N^2/[g(m^2 + 1/4H^2)]$.

4. Thermally forced tropical circulation: Two idealized cases

Some simple analytical solutions to a forced shallow-water system with a single positive equivalent depth were given by Matsuno (1966) and Gill (1980). With prescribed linear damping, the steady solution to Eqs. (2.8a)–(2.8c) is characterized by the Kelvin signal that decays to the east of the heat source and by the Rossby signals that decay to the west of the heat source. The zonal distance that the signals can reach is characterized by the product of the damping timescale and the zonal group speed. Since the propagation speed of the Kelvin signal is three times larger than that of the fastest Rossby signal, the response to the east of the heat source extends about three times farther than that to the west of the heat source. Since the zonal group speeds of the Kelvin and Rossby signals are determined by the equivalent depth of the shallow-water system, in a zonally cyclic domain Gill's solution can be an approximate solution only for sufficiently small equivalent depth, sufficiently large damping, or both. Otherwise, the eastward and westward propagating signals extend around the circumference of the earth and interfere with each other.

For vertically isolated heating, the vertical structure of the response cannot be resolved by a single vertical mode. Hence, the original three-dimensional system must be decomposed into an infinite set of shallow-water systems. For each shallow-water system, the horizontal structure of the response to a heat source of a given horizontal structure is different since the equivalent depth of each vertical mode is different. In addition, the amplitude of the response is also affected by how much of the input energy goes to each mode. Since the overall solution is the summation of the contributions from all vertical modes, the projection of the vertical heating

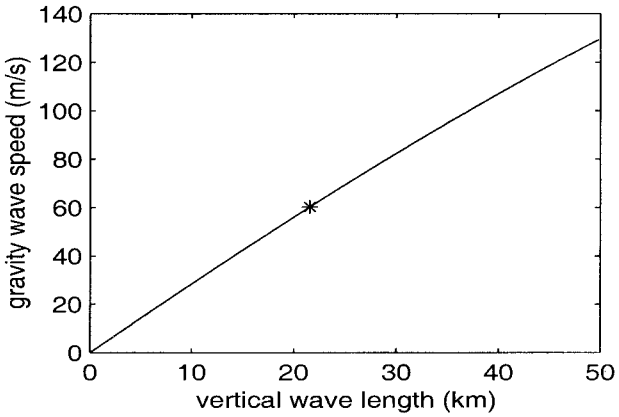

FIG. 1. The plot of the gravity wave speed against the vertical wavelength for a baroclinic mode in an isothermal atmosphere of 300 K. The point, as shown by the asterisk (*), corresponds to the gravity wave speed of 60 m s^{-1}.

profile onto the vertical eigenmodes becomes one of the key factors in characterizing the structure of the thermally forced response.

To facilitate the discussion of which vertical modes contribute significantly in the response to prescribed heating, we first introduce the vertical wavelength l of a baroclinic (internal) mode:

$$\left(\frac{2\pi}{l}\right)^2 = m^2 = \left(\frac{N^2}{gh_m} - \frac{1}{4H^2}\right). \tag{4.1}$$

Equation (4.1) gives the relationship between the vertical wavelength l and the equivalent depth h_m of the corresponding shallow-water system. Figure 1 plots the square root of the equivalent depth $\sqrt{gh_m}$ (the horizontal gravity wave speed of a vertical mode) as a function of the corresponding vertical wavelength l for an isothermal atmosphere of temperature 300 K. (The corresponding scale height H is 8.785 km and the buoyancy frequency squared N^2 is 3.2×10^{-4} s^{-2}.) The point shown by the asterisk (*) corresponds to the mode with gravity wave speed of 60 m s^{-1}. The vertical wavelength corresponding to that equivalent depth is smaller in this case than that in Gill (1980) since we choose an isothermal atmosphere that has a relatively larger N^2.

For simplicity, we assume that the heating rate $\tilde{Q}$ in Eq. (2.9) has the separable form $P(z)S(x, y)$. Then, we obtain

$$F_m(x, y) = F(m)S(x, y), \tag{4.2}$$

where $F(m)$ is the projection of $P(z)$ onto the vertical eigenfunction $V_m(z)$. The expression of $P(z)$ in terms of the vertical eigenfunctions is

$$P(z) = F_e e^{-(z/2H)} + \sqrt{\frac{2}{\pi}} \int_0^\infty F_i(m)\left(\cos mz - \frac{1}{2Hm}\sin mz\right) \times \frac{2Hm}{\sqrt{4H^2m^2 + 1}}\, dm, \tag{4.3}$$

where F_e is the projection of $P(z)$ onto the external mode,

$$F_e = \frac{1}{H}\int_0^\infty P(z)e^{-(z/2H)}\, dz, \tag{4.4a}$$

and $F_i(m)$ is the projection of $P(z)$ onto an internal mode,

$$F_i(m) = \sqrt{\frac{2}{\pi}} \int_0^\infty P(z)\left(\cos mz - \frac{1}{2Hm}\sin mz\right) \times \frac{2Hm}{\sqrt{4H^2m^2 + 1}}\, dz. \tag{4.4b}$$

The Parseval's theorem states that the energy E is given by

$$E = \int_0^\infty |P(z)|^2\, dz \approx \int_0^\infty F^2(m)\, dm = \int_0^\infty \frac{2\pi F^2(l)}{l^2}\, dl, \tag{4.5}$$

where the "≈" indicates that the contribution from the external mode is neglected since it accounts for little of the whole integral when large-scale convective heating is considered. The variable $F^2(m)$ is often called the power spectrum, and here, $2\pi F^2(l)/l^2$ is called the spectral energy density with respect to vertical wavelength l. *The relative importance of the different modes in accounting for the overall response can be quantified by these two quantities.*

The heat source considered in this paper is due to the large-scale persistent precipitation in the Tropics (e.g., the large-scale convective heating over the Maritime Continent near Indonesia). Recent investigations based on Tropical Oceans and Global Atmosphere Coupled Ocean–Atmosphere Response Experiment (TOGA COARE) field experiments revealed more insight on the vertical structure of the convective heating in the western tropical Pacific. Among these studies, Mapes and Houze (1995) provided a detailed description of diabatic divergence based on radar observations in the COARE intensive flux array region. Within measurement error, as Mapes and Houze (1995) pointed out, the diabatic divergence may quite accurately approximate the divergence driven by the bulk heating. However, since the vertical structure of the tropical heating related to cumulus convection varies with time and location (e.g., Frank and McBride 1989), it is difficult to find an exact representation of a realistic large-scale tropical heat source in the Tropics. Furthermore, since one of the main goals of this study is to understand the relationships between the vertical structure of heating and the forced circulation rather than to simulate the realistic response of atmosphere to a realistic heating, simple representations of the vertical structure of heating may better help us to accomplish that goal. Thus, here, we simply follow Hartmann et al. (1984) and consider two

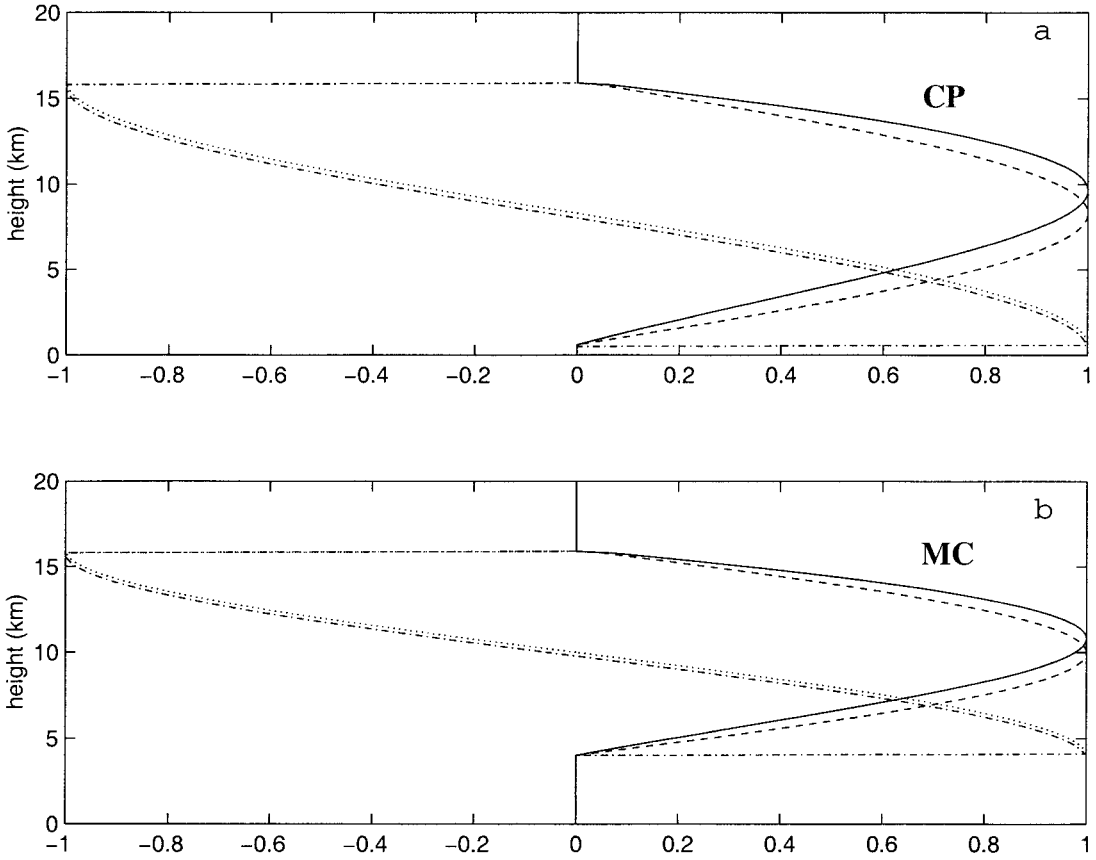

FIG. 2. The normalized vertical heating profiles in the analytical study for two idealized cases: (a) the convective plume (CP) heating case and (b) the mature cloud (MC) cluster heating case. In (a) and (b) the solid line represents the vertical structure of the external heating rates J, the dashed line represents the vertical structure of the mass weighted external heating rate Q, the dash–dotted line is the vertical structure of the forcing function $\tilde{Q}$ defined in Eq. (2.9), and the dotted line is $P(z)$ given in Eq. (4.7).

different heating profiles: 1) an idealized profile representing the total heating produced by CP alone (and 2) an idealized profile representing the total heating produced by strataform precipitation typical of an MC. Although the long-term mean heating has a similar vertical structure to that of CP (Mapes and Houze 1995), the MC profile is examined to show that the vertical structure of the heating is one of the key factors in determining the three-dimensional structure of the atmospheric response to a prescribed heating. The two heating profiles are expressed as

$$J(z) = \begin{cases} 0 & z \geq z_t, \\ e^{z/2H} \sin\left(\dfrac{z - z_b}{z_t - z_b}\pi\right) & z_b < z < z_t, \\ 0 & z \leq z_b, \end{cases} \quad (4.6)$$

where z_t is the cloud top (somewhere close to the tropopause) that is assumed to be at 16 km. The bottoms of the heating level z_b are assumed to be at 0.6 and 4 km for the CP and the MC, respectively. The normalized vertical structures of J, Q, and $\tilde{Q}$ are plotted in Fig. 2. The contribution to $\tilde{Q}$ by the term with the scale height H in Eq. (2.9) is small (see Fig. 2). Hence, for simplicity, we take

$$P(z) \propto \left(\frac{\partial}{\partial z} - \frac{1}{2H}\right)(\rho_0^{1/2} J) \propto \left(\frac{\partial}{\partial z} - \frac{1}{2H}\right) Q$$
$$\approx \begin{cases} 0 & z \geq z_t, \\ \cos\left(\dfrac{z - z_b}{z_t - z_b}\pi\right) & z_b < z < z_t, \\ 0 & z \leq z_b. \end{cases} \quad (4.7)$$

From Eqs. (4.4b) and (4.7), we obtain

$$F(m) = -\frac{m}{m^2 - n^2} \frac{1}{\sqrt{1 + 4H^2m^2}} \sqrt{\frac{2}{\pi}} \times [2Hm(\sin mz_t + \sin mz_b) + \cos mz_t + \cos mz_b], \quad (4.8)$$

where $n = \pi/(z_t - z_b)$.

Equations (4.3) and (4.5) are used to calculate pro-

jections $P(z)$ of the heating functions onto internal modes for these two cases; solutions are shown in Fig. 3. In both cases, the spectrum of the heating is dominated by the modes with vertical wavelength greater than 10 km; the modes of strong, vertically wavy structures (small vertical wavenumber) do not contribute much to the forced response. The spectral energy distribution with respect to the vertical wavenumber is very sensitive to the location of the cloud base. For the MC case, the energy is dominated by the modes with a vertical wavelength of around 14 km (which corresponds to the gravity wave speed of 40 m s^{-1}), while for the CP case, more than 70% of the energy is carried by the modes of the vertical wavelength greater than 18 km.

These differences are significant for the interpretation of the forced response. Gill (1980) has already shown that for a shallow-water system, the amplitude of the zonal velocity to the east of the heating can be expressed as

$$u(x + \Delta x) = u(x) \exp(-\alpha \Delta t) = u(x) \exp\left(-\frac{\Delta x}{cT}\right), \quad (4.9)$$

where α is the Rayleigh friction rate, T is the timescale of Rayleigh friction, and c is the gravity wave speed of the shallow-water system. Since modes of different vertical wavelengths propagate at different speeds, under the same linear dampings, one could expect that a signal associated with larger vertical wavelengths decays slower in the zonal direction and would be detected farther away from the heat source than the signal with the shorter vertical wavelength. For this reason, we anticipate that the forced response to CP decays slower in the zonal direction than the response to MC, which results in different horizontal structures.

The drawback of a single mode approach used in Gill (1980) is also clear from Fig. 3. If the spectral energy density $2\pi F^2(l)/l^2$ is highly concentrated around some mode, it may be appropriate to approximate the response by just considering that single mode. However, Fig. 3 shows that the spectral energy is distributed broadly over vertical wavelength and is very sensitive to the vertical structure of the heating. Since the contribution from a single mode at a given height is dependent on the height, in general, the overall solution at a given height exhibits height dependent horizontal decay rates. Such a result is clearly in contrast to the Gill solution in which the horizontal decay rate is vertically uniform.

It should be noted here that the heating discussed in this paper is persistent and in a fixed location, whereas the real heating in the western tropical Pacific and the Indian Oceans has a significant component that varies on intraseasonal timescale and moves eastward at a speed of 8 m s^{-1}. However, the three-dimensional structure discussed in this section is still applicable to the response of the atmosphere to a time-dependent, slow-moving heat source since the majority of the forced signals propagate with a speed of about an order faster than the moving speed of the heat source.

5. Numerical experiments

In this section, we analyze the results from two idealized numerical experiments in which the vertical structure of the heating is prescribed as either CP or MC. We examine the circulation patterns associated with both cases and determine to what extent the model results can be explained by the linear theory presented in the previous sections.

a. The model and experiments

The model we use is the dry version of the primitive equation model developed by Saravanan and McWilliams (1995) and was previously used extensively (Wu et al. 2000). The model assumes that the planetary surface has no topography and that the solutions are calculated using spectral methods with a vertical pressure coordinate.

The divergent shallow-water mode with equivalent barotropic vertical structure is excluded from the model by a rigid lid. Such an artificial lid produces the spurious free oscillations that are resonant when the atmosphere is forced (Lindzen et al. 1968). In general, an atmosphere bounded by a lid does not properly respond to oscillations that propagate vertically since a rigid lid leads to a spurious reflection of wave energy that does not occur in a semi-infinite atmosphere. To avoid this drawback, a common approach is to incorporate strong damping at the top of the models to absorb vertically propagating waves (e.g., Hendon and Salby 1996). This approach was justified by Geisler and Stevens (1982), who, among others, demonstrated that in the presence of dissipation, forced low-frequency waves are damped before they reach the lid, while at high frequencies, the artificial lid does reflect the wave energy. The approach was further explained by Wu et al. (1999), who showed that the low-frequency waves have much smaller vertical group velocities than high-frequency waves and propagate shorter distances before they are damped.

The Rayleigh friction rate and the Newtonian cooling rate are taken to be $\alpha^{-1} = 2.5$ days everywhere. These damping rates are close to the values used in Gill (1980) when a gravity wave speed of 60 m s^{-1} is selected and are comparable to those used in other models (e.g., Geisler 1981). The model results to be discussed are not qualitatively dependent on the values of the damping rates unless they are very small. The model results for the values of dissipation used also show that the solutions are almost independent of the artificial lid as long as the lid is well above the top of the isolated heat source.

The vertical resolution is set to 60 equal layers of pressure thickness. The horizontal resolution is T21,

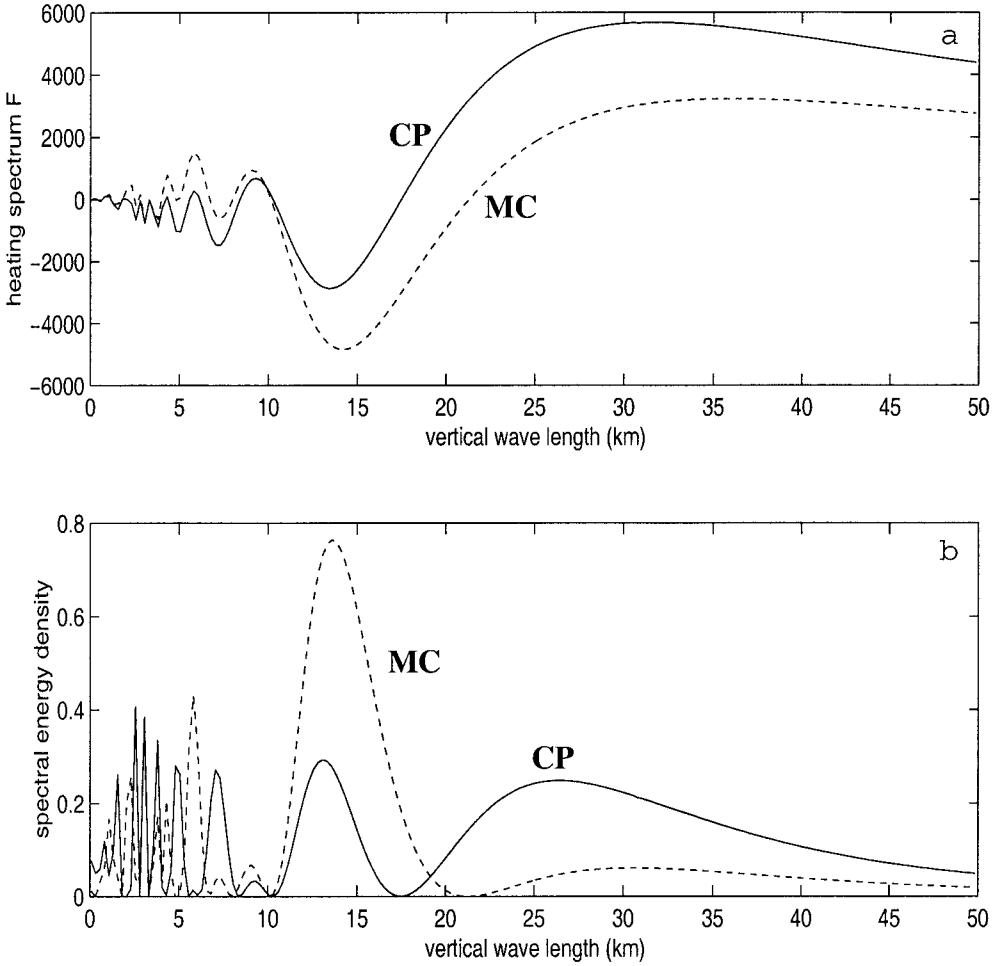

FIG. 3. The projections of the external forcing functions (the dotted lines in Fig. 2) onto the vertical eigenfunctions. (a) The spectra $F(l)$ and (b) the spectral energy density of the heating as a function of vertical wavelength l. The solid lines are for the CP case and the dashed lines are for the MC case.

which corresponds to 64 grid points zonally and 33 grid points meridionally.

To directly compare numerical results to the theoretical results in section 4, we take the resting atmosphere to be isothermal at 300 K and exclude an explicit boundary layer. The lower-boundary conditions is $w^* = 0$.

The heat source is prescribed to be

$$Q = \exp[-(\lambda - \lambda_0)^2/\lambda_L^2] \exp(-\phi^2/\phi_L^2)F(p), \quad (5.1)$$

where λ is longitude, λ_0 is reference longitude with a value of 93°E, $\lambda_L = 20°$, ϕ is latitude, and $\phi_L = 11°$. The variable $F(p)$ is calculated from the vertical heating profiles as expressed by Eq. (4.6) and plotted in Fig. 2. The maximum heating rate is set by requiring the vertically integrated heating to be equivalent to the amount of latent heating provided by 10 mm of precipitation per day (corresponding to 2.5 K day^{-1}). The heating amplitude is not crucial in this study; numerical experiments show that the three-dimensional structure of the response is not sensitive to the amplitude of the heating as long as the maximum heating rate corresponds to less than 20 mm day^{-1} of precipitation. However, the amplitude of the response is approximately proportional to the maximum heating rate. Hence, the modeled response is essentially linear.

The global kinetic energy and the global perturbed potential energy for both cases approach their approximate steady states in a couple of model weeks. We therefore run both model experiments for 100 model days to approach an approximate equilibria.

b. Results

In the previous sections, it is shown that the signals carried by modes of different vertical wavelengths propagate horizontally at different speeds. The larger the vertical wavelength of a mode, the faster the signal carried by this mode can propagate. The theoretical gravity wave speed limit for the baroclinic mode in an isothermal atmosphere of 300 K is 314 m s^{-1} (which is

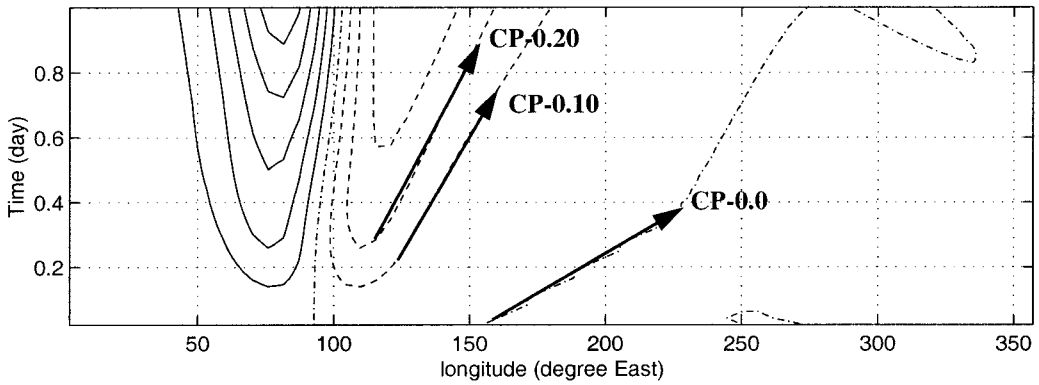

FIG. 4. The zonal velocity along the equator for the CP case at 810-hPa level throughout the first day of the spinup processes. The contour interval is 0.10 m s^{-1}, the solid lines represent westerlies, the dashed lines represent easterlies, and the dash–dotted lines are zero contour lines. The meaning of the superposed bold arrows are discussed in the text.

also the sound wave and Lamb wave speed), as indicated by Eq. (4.1) when the vertical wavenumber is taken to be zero. From Eqs. (4.5) and (4.8), we expect that contributions by modes with extremely large vertical wavelength are very small for the MC and CP heating profiles. Hence, we expect the largest wave speed detected in the numerical experiments would be somewhat smaller than 314 m s^{-1}.

Figure 4 plots the zonal velocity along the equator at 810-hPa level for the CP case at the equator throughout the first day of the integration. In the early stages of spinup, the amplitude of the forced signal is much smaller than that of the equilibrium (steady) solution at any given location; hence, the damping plays a relatively insignificant role and the forced signal propagates almost freely. Although the ensemble signal of a certain

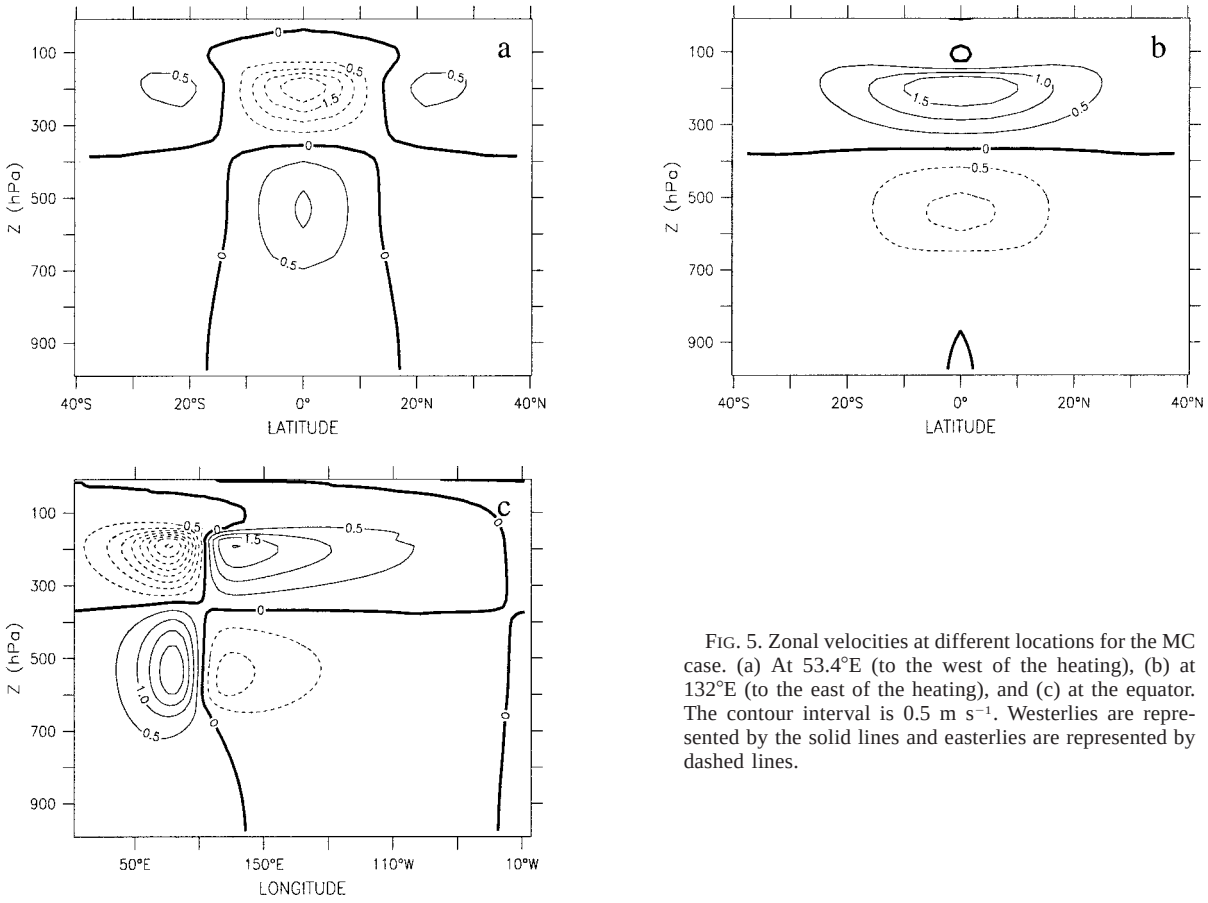

FIG. 5. Zonal velocities at different locations for the MC case. (a) At 53.4°E (to the west of the heating), (b) at 132°E (to the east of the heating), and (c) at the equator. The contour interval is 0.5 m s^{-1}. Westerlies are represented by the solid lines and easterlies are represented by dashed lines.

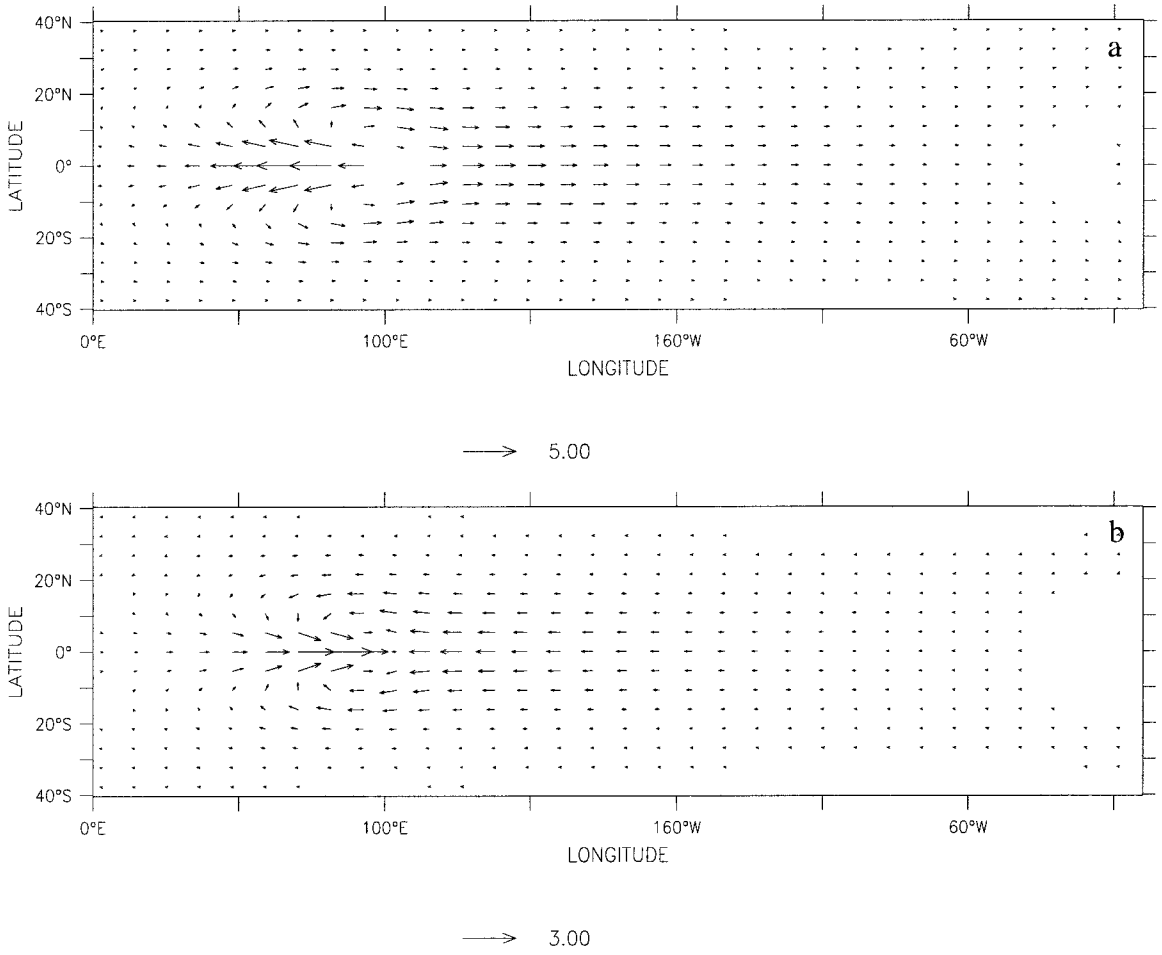

FIG. 6. The horizontal velocities at (a) 190 hPa and at (b) 560 hPa for the MC case. The scaling vectors are shown under each panel. The unit of the velocity is meters per second.

amount of kinetic energy, which includes the contribution from all the modes, disperses, it may still approximately propagate at a constant speed because the part of the signal that propagates relatively faster (slower) and disperses to the front (rear) is compensated by the same amount of signal of the same speed from the rear (front) as long as the heating rate is a constant. Therefore, the slopes of the bold arrows in Fig. 4, which are tangent to isotachs, can approximate propagation speeds of the signals of different kinetic energy. Furthermore, one can obtain the propagation speed of the fastest mode in the model by tracking an incipient front as it travels along the equator. In this case, the speed of the fastest eastward propagating mode can be determined by tracking the zero contour of zonal wind, which indicates that the fastest mode travels at about 250 m s^{-1}. This speed is comparable to the analytical value (314 m s^{-1}) and does not depend on details of the heating profile. From Eq. (4.8) and Fig. 3b, we can infer that contributions from the modes with gravity wave speeds greater than 250 m s^{-1} are negligible. Hence, the numerical model used for this study is capable of simulating the proposed relationship between the vertical structure of the convective heating and the three-dimensional structure of the forced circulation in a vertically semi-infinite atmosphere.

The general features of the steady solution for the MC case are shown in Figs. 5 and 6. The response is mainly confined in the vertical to where the heating is located (Fig. 5); above and below the heating, the response is quite weak. The zero zonal wind contour is located around the 370 hPa, which is much lower than the maximum heating level of about 270 hPa. In the meridional direction, the response is confined mainly to the Tropics. To the west of the heat source (Fig. 5a), the upper troposphere is dominated by easterlies centered at the equator with narrow bands of relatively weak westerly wind on the poleward flanks. The zonal wind in the lower troposphere is opposite to that in the upper troposphere and has a relatively small amplitude (see also Fig. 6). To the east of the heat source (Fig. 5b), the lower troposphere is dominated by easterlies and the upper troposphere is dominated by westerlies, and the zonal winds in upper troposphere have relatively larger

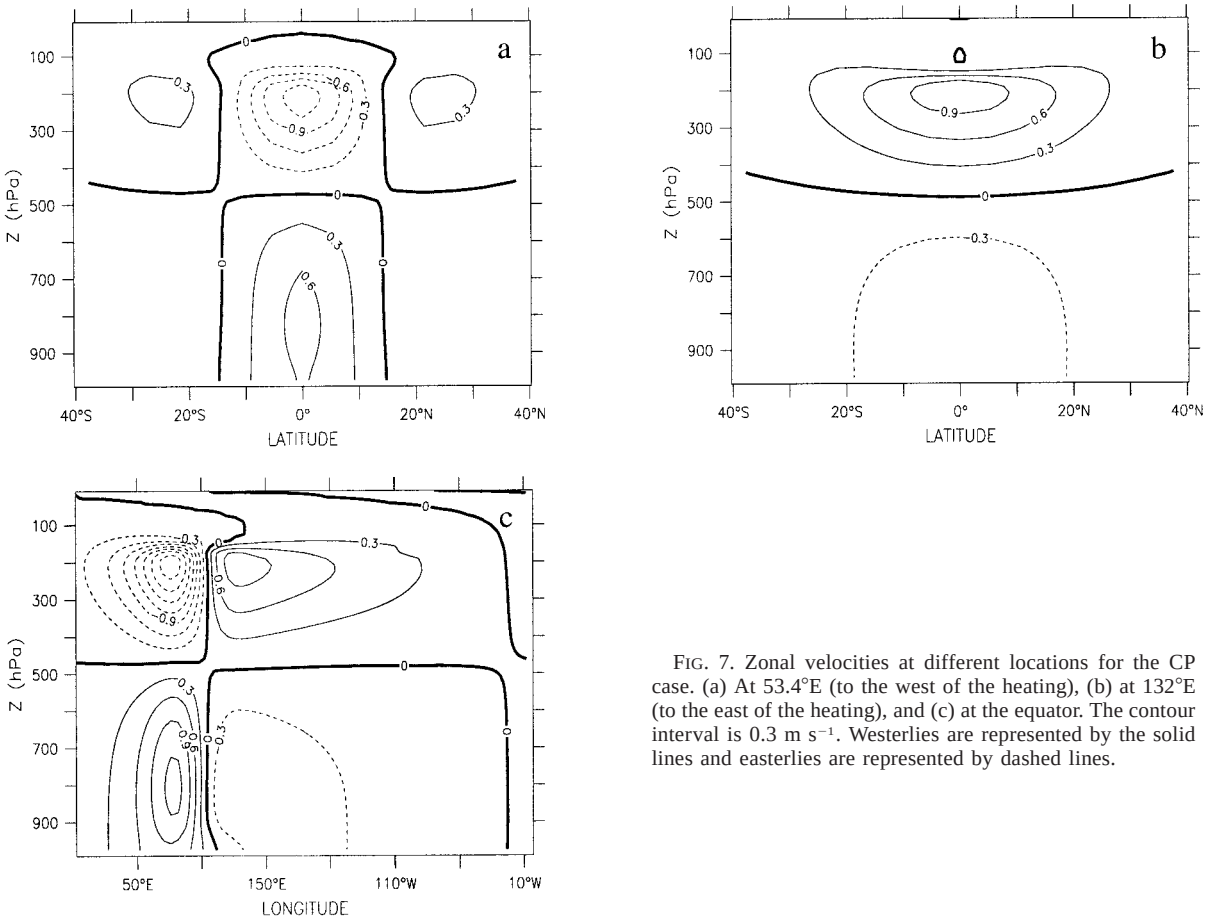

FIG. 7. Zonal velocities at different locations for the CP case. (a) At 53.4°E (to the west of the heating), (b) at 132°E (to the east of the heating), and (c) at the equator. The contour interval is 0.3 m s^{-1}. Westerlies are represented by the solid lines and easterlies are represented by dashed lines.

amplitude. The maximum zonal wind level is at about 190 hPa in the upper troposphere and 560 hPa in the lower troposphere (see Fig. 5c). The forced signal decays zonally away from the heat source, with a much larger decay rate to the west of the heating (Fig. 6). Although the horizontal structure of the wind field at both levels is similar to that shown in Gill (1980), the zonal decay scale is smaller at 560 hPa than at 190 hPa (see Fig. 5c), indicating that the contributions from various modes are different at different levels.

The steady circulations for the CP case are shown in Figs. 7 and 8. In Fig. 7, note that the zero zonal wind level is at about 450 hPa, which is again far below the maximum heating level. Above the heating top, the response is again very small; however, the response now extends below the heating and to the ground. The maximum zonal wind level is at about 210 hPa in the upper troposphere and 810 hPa in the low troposphere (see, Fig. 7c). The horizontal structure of the wind field at these two levels is shown in Fig. 8. Unlike the MC case, in the CP case, the zonal decay rate at the upper and lower maximum wind levels are very similar. This difference is more obvious in Fig. 9, where the zonal velocity from 137.8°E to 300.9°W along the equator and along 10.7°N and at different levels are shown for both cases. It is clear that the zonal decay rate is dependent on heights, latitudes, and the structure of the heating profile.

To quantitatively describe these differences, we introduce the concept of effective gravity wave speed. An effective gravity wave speed $\overline{c}$ is defined as the gravity wave speed of a hypothetical linear shallow-water system that best approximates the multimode system at a given location. From Eq. (4.9), an local estimate of $\overline{c}$ is

$$\overline{c} = \frac{\Delta x}{T \ln\left[\dfrac{u(x)}{u(x + \Delta x)}\right]}, \tag{5.2}$$

where Δx is the zonal distance between neighboring grid boxes where u is measured and T is the damping timescale of Rayleigh friction. Figure 10 shows contours of the gravity wave speed to the east of the heating at levels where the wind is an extreme in the vertical. It is clear that the effective gravity wave speeds are generally much larger in the CP case than in the MC case. The effective gravity wave speeds are different at upper troposphere and lower troposphere, but this difference is

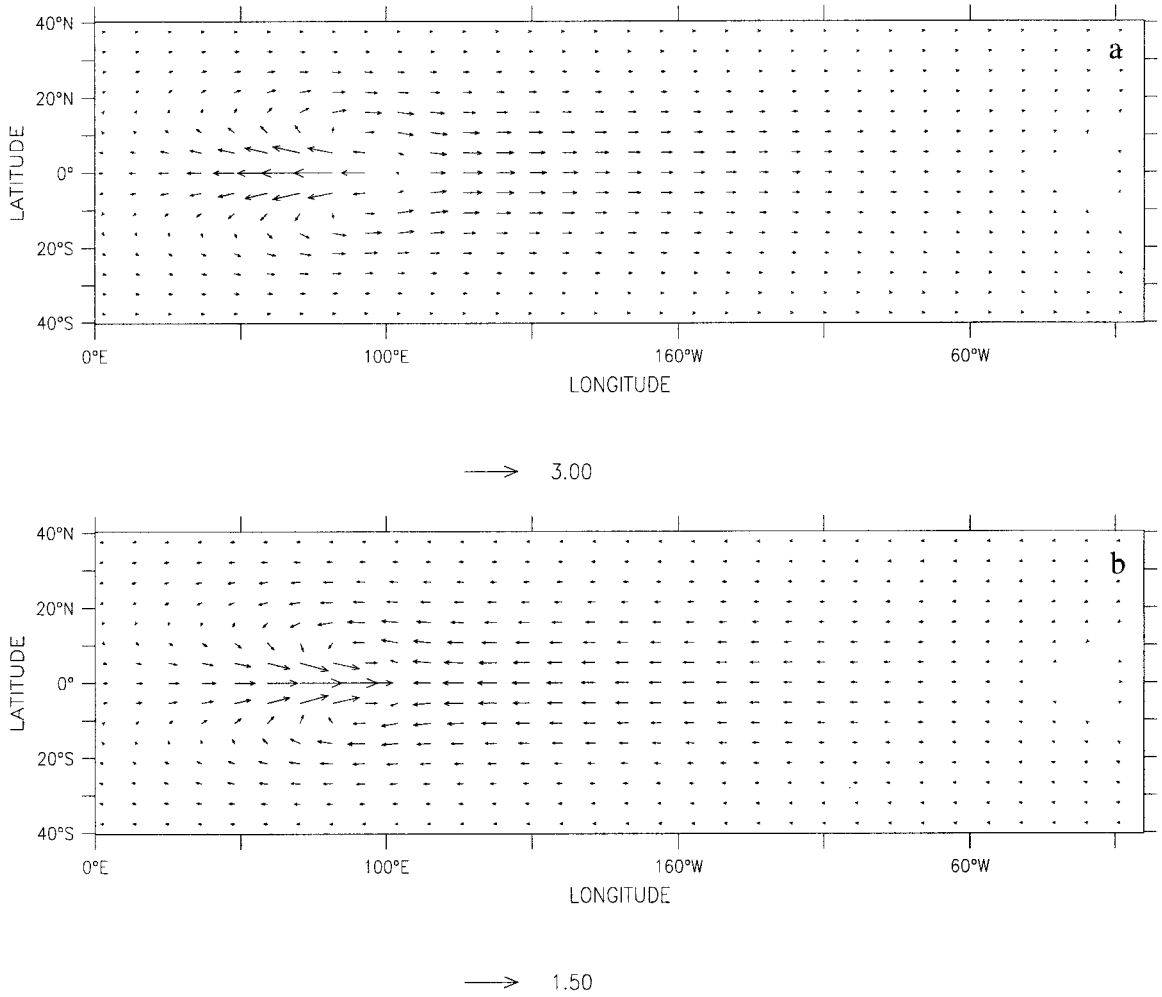

FIG. 8. The horizontal velocities at (a) 210 hPa and at (b) 810 hPa for the CP case. The scaling vectors are shown under each panel. The unit of the velocity is meters per second.

more notable in the MC case. At every level, the effective gravity wave speed increases with increasing latitudes from the equator because the slower wave modes have experienced their turning latitudes, leaving only the faster (larger vertical wavelength) modes to carry the forced signal to the higher latitudes. Regardless of the type of heating, the effective gravity wave speed also becomes larger to the east until the longitude is reached where the Rossby wave signal significantly contributes.

As the forced signal propagates to the east, the part carried by the Kelvin solutions with relatively smaller gravity wave speed are easily damped, leaving the faster Kelvin solutions to dominate the response. This is further shown in Fig. 11, where the vertical profiles of the zonal wind and their spectral energy densities with respect to the vertical wavelength are plotted for both cases. In Figs. 11a and 11b, we see that the vertical scale of the response becomes larger toward the east. Figures 11c and 11d plot the spectral energy densities for the mass-weighted zonal velocities for the CP case and the MC case, respectively. By comparing the solid line in Fig. 11c with the solid line in Fig. 3b, we see that the spectral energy density of the mass-weighted zonal velocity immediately east of the heating resembles the spectral energy density of the heating. But at 149.1°W, the modes with vertical wavelengths smaller than 10 km have diminishingly small amplitude. Farther to the east at 81.8°W, only the modes with vertical wavelengths greater than 16 km have survived. Similar decaying property also holds for the MC.

The difference between the maximum heating level and the zero wind level in each case as well as the three-dimensional structure of the zonal decay rate in each case and the qualitative differences in the structure of the wind field below the heating in the two different cases clearly indicates that a single vertical mode approximation is incapable of approximating the qualitative three-dimensional structure of the response to tropical heating.

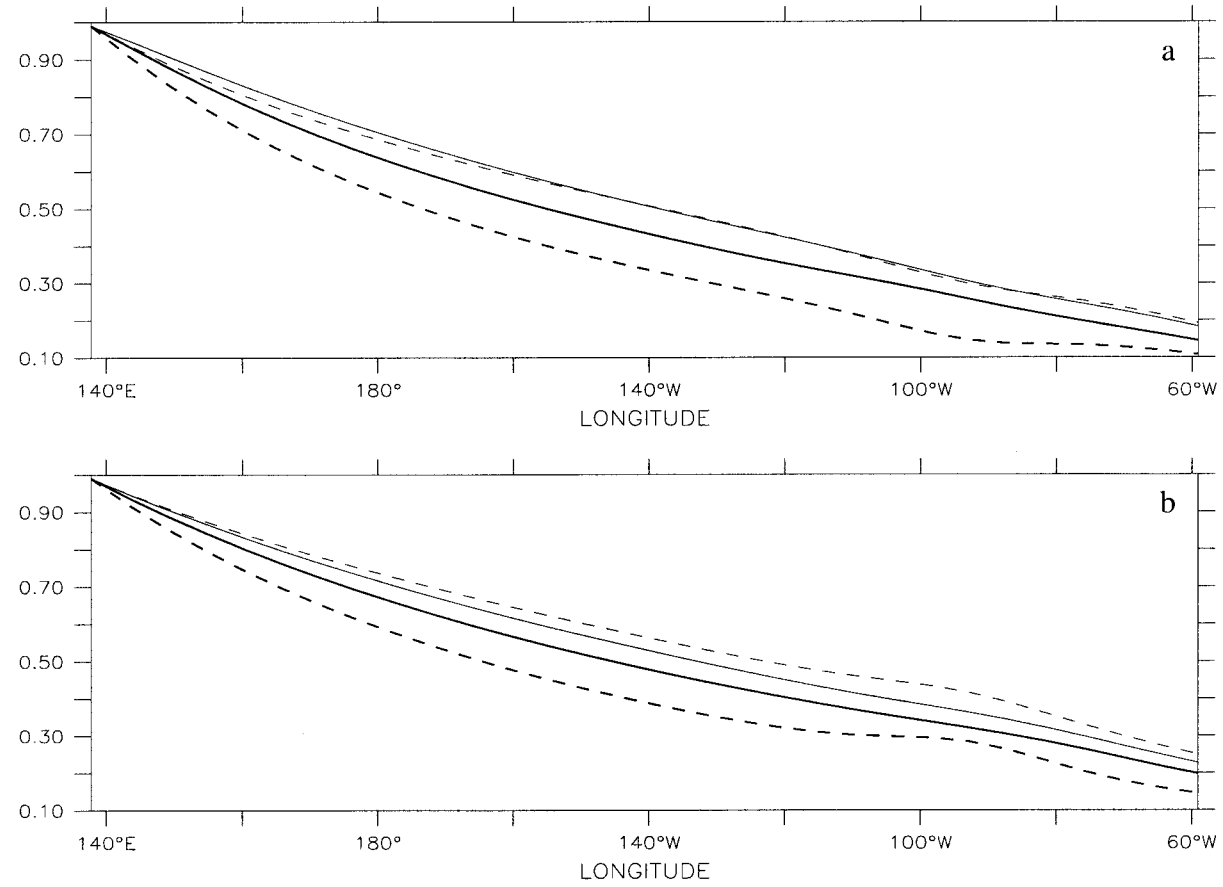

FIG. 9. The scaled zonal velocities along (a) the equator and along (b) 10.7°N relative to the zonal velocities at 137.8°E at the same latitude and height. In (a) and (b) the thin solid line and thin dashed line correspond to the heights of 210 and 810 hPa for the CP case, respectively; the bold solid line and bold dashed line correspond to the heights of 190 and 560 hPa for the MC case, respectively.

6. Summary and discussion

We have examined the three-dimensional structure of the response to an isolated, steady, large-scale heat source in the Tropics using both analytical arguments and numerical simulations of a dry primitive equation model of the atmosphere. In the analytical part of the study, we separated the linear equations into a homogeneous vertical structure equation and a set of forced shallow-water equations. By solving the vertical eigenvalue–eigenfunction problem in a vertically semi-infinite domain, we obtained the eigenvalues and a complete set of vertical eigenfunctions, which include a discrete barotropic mode and a continuous spectrum of baroclinic modes. These vertical eigenfunctions were used to decompose two different vertical heating profiles: 1) a profile that represents the total heating produced by an ensemble of deep convective plumes (the CP case) and 2) a profile that represents the net heating produced by the aggregate heating due to a mature tropical cloud cluster (the MC case) where stratiform precipitation happens. By examining the spectral energy density of the heating profiles and considering the steady solution to the shallow-water system given by Gill (1980), the three-dimensional structure of the response to each heating profile was analyzed. To verify the analytical results, we carried out the corresponding numerical experiments.

Our results from both the analytical and the numerical simulations are consistent in showing why the vertical structure of the heating is fundamental to determining the structure of the response to a thermal source, which has long been recognized (e.g., Geisler 1981; Hartmann et el. 1984; Lau and Peng 1987; Sui and Lau 1989; Wang et al. 1996) but not well explained. Since the projection of a prescribed heat source onto the vertical modes is sensitive to the vertical structure of that heat source, the contributions from different vertical modes to the responses of the tropical atmosphere to the heatings of different vertical structures are different. Furthermore, since the spectrum of the modes that contribute to the overall solution, in general, is very broad, under the same damping, the signals carried by different modes possess different propagation speeds and different spatial decay rates. Hence, the relative contributions of various modes to the overall solution are different at different locations; the relative contribution to the net

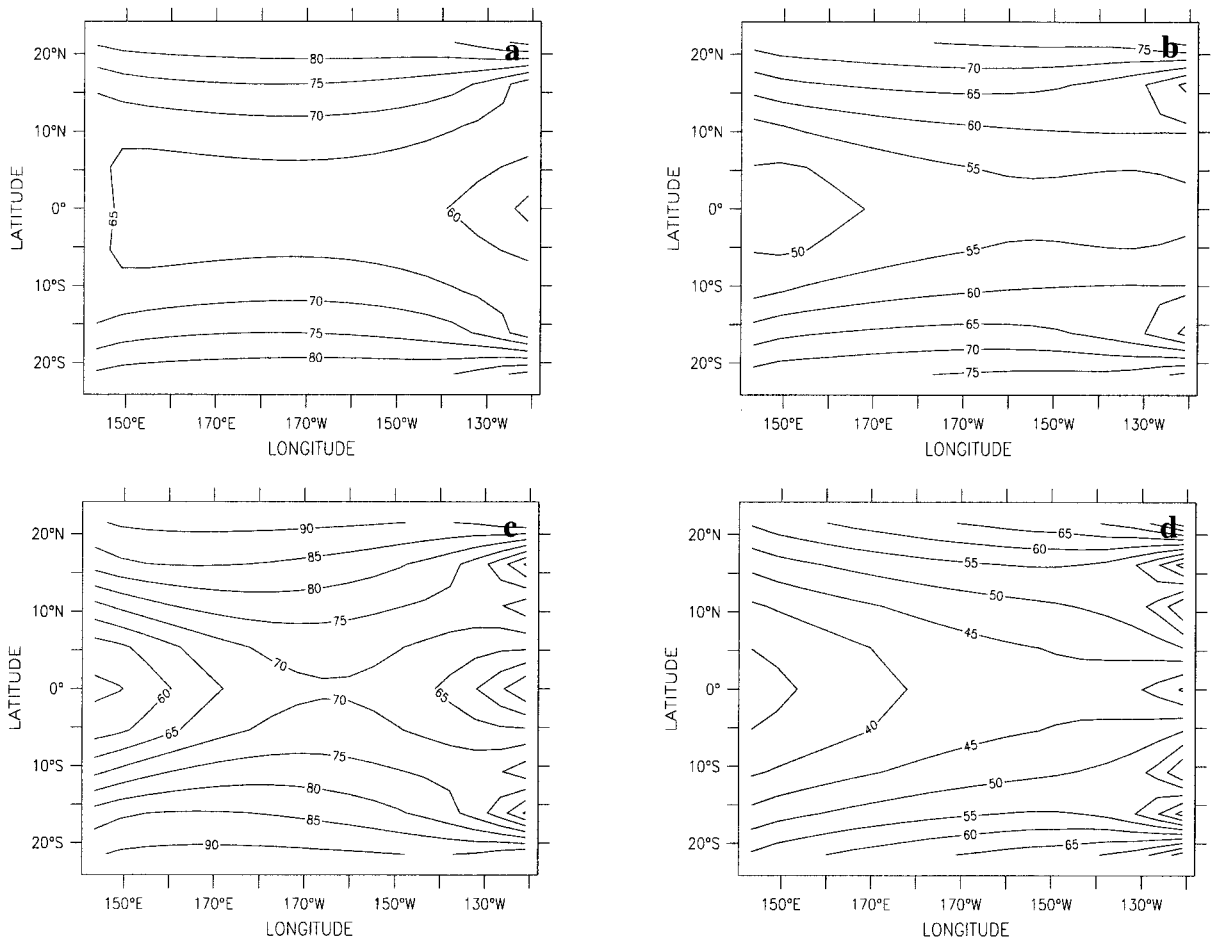

FIG. 10. Effective gravity wave speed at different levels for the CP case [(a) at 210 hPa and (c) at 810 hPa] and for the MC case [(b) at 190 hPa and (d) at 560 hPa]. The contour interval is 5 m s^{-1}.

solution due to modes of large vertical wavelengths increases as the ensemble signal propagates farther away from the heating.

Compared to the MC heating, the CP heating is deep and projects onto vertical eigenfunctions with relatively larger equivalent depth, so the forced signals propagate away from the heat source much faster than those forced by the MC heating. Hence, the averaged spatial decay rate of the signals forced by the convective plume heating is significantly smaller than the decay rate of the signals in the MC case and, as a result, the propagating signals can be detected farther away from the heat source in the CP case.

One of the questions to be answered by this study is whether the Gill model can approximate the general feature of the circulations forced by deep convective heating. It is easy to show, from Eq. (4.8), that even for a heat source with a perfect sinusoidal heating rate from the surface to the tropopause, as was idealized in the Gill model, the projection of heating onto the spectrum of the vertical is quite broad. Hence, Gill's assumption that the important contribution to the solution comes mainly from a mode with an inverse vertical wavenumber of the same scale as that of the forcing function was questionable. Our numerical results further showed that the zero zonal wind level is far below the maximum heating level. This implies that a single vertical mode model is incapable of approximating the forced response throughout the Tropics. The theoretical explanation is as follows: since different modes have different vertical structures, the relative contribution from each mode is different at different heights. Hence, it is extremely difficult to select a single suitable equivalent depth for a shallow-water system to approximate the three-dimensional structure of the response to a given heating. This argument is further confirmed by the model experiments through examining the effective gravity wave speed.

An interesting feature of the tropical atmosphere that has not been well explained is the zonal acceleration of intraseasonal signals to the east of the date line when they propagate eastward. Such a feature was first recognized by Madden and Julian (1972). In Fig. 4 of their seminal paper, they showed that the distances between the isograms of phase increase eastward in the

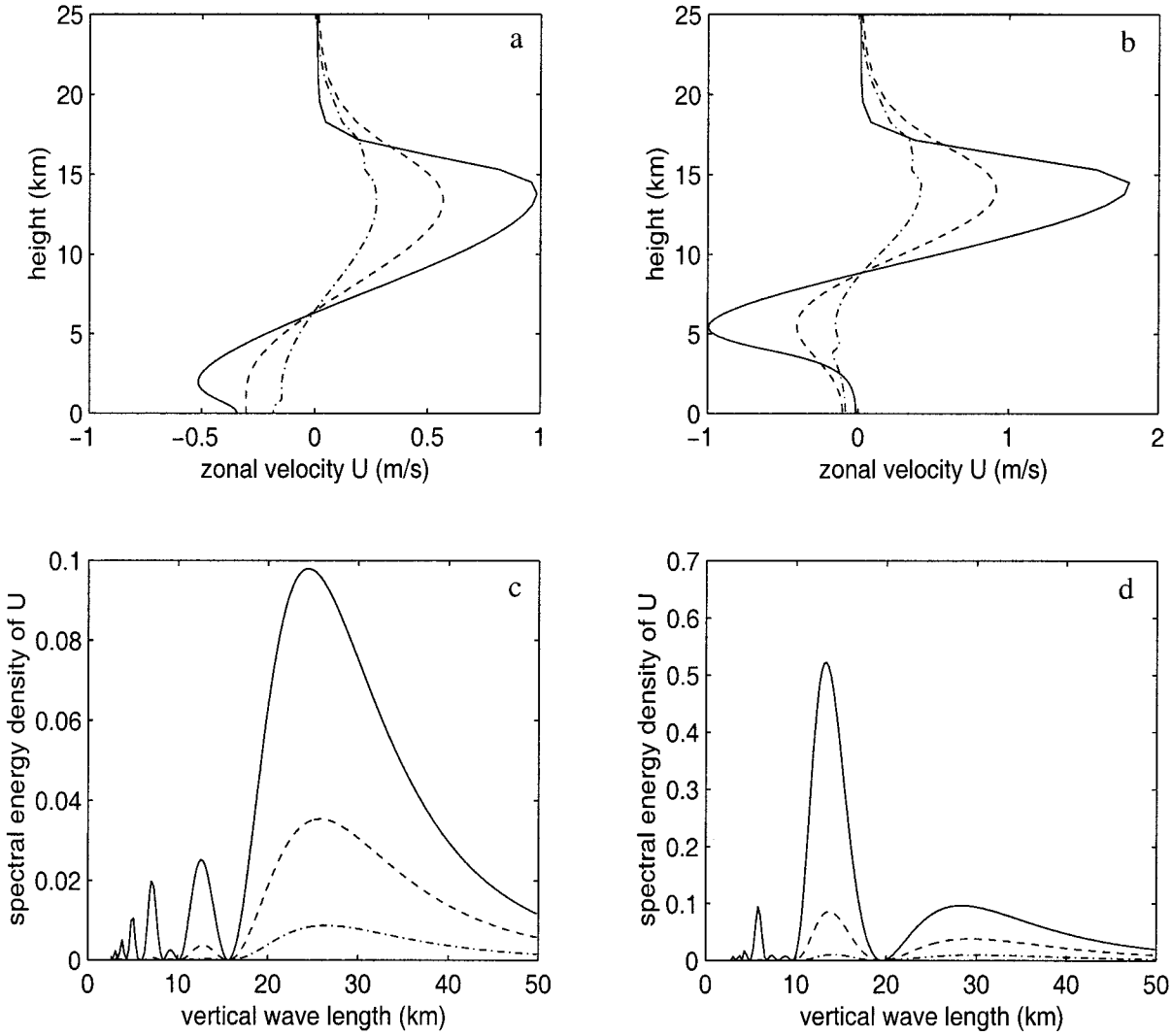

FIG. 11. The zonal velocities [(a) for the CP case and (b) for the MC case] and their spectral energy densities [(c) for the CP case and (d) for the MC case] in the spectral space for the mass-weighted zonal velocities at different longitudes at the equator. Solid lines are for 143.4°E, dashed lines are for 149.1°W, and dash–dotted lines are for 81.8°W.

equatorial tropical Pacific, indicating that the ensemble signals propagate faster and faster away from the regions where the main intraseasonal variation of convective heating happens. More studies (e.g., Milliff and Madden 1996) detected the fast, eastward-moving signals with a speed faster than 30 m s^{-1} in the equatorial troposphere of the eastern Pacific on the intraseasonal timescale, while the propagation speed of the disturbances to the west of 180° is about 8 m s^{-1}. Our result that the relative contribution to the net solution due to fast propagating modes increases as the ensemble of the forced signals propagates farther away from the heating (indicated by the zonal increase of the effective gravity wave speed) provides a partial explanation for such an observational feature. However, further examination is necessary to see whether that observed phenomenon is due solely to the linear response to slowly moving heat sources.

Acknowledgments. We are grateful to E. Harrison and S. Hankin of NOAA/PMEL for providing us with FERRET, a very useful diagnostic and graphic program. We also thank two anonymous reviewers for suggestions that led to significant improvements in the manuscript. This work and publication was funded by a grant from the Joint Institute for the Study of the Atmosphere and Ocean (JISAO) at the University of Washington under NOAA Cooperative Agreement NA67RJ0155, Contribution 587. The views expressed herein are those of the authors and do not necessarily reflect the views of NOAA or any of its subagencies.

APPENDIX

Spectral Expression of δ Function

The spectral representation of an operator $L = -d^2/dx^2$ can be expressed in terms of the Green's function defined by Eq. (3.4)

$$\lim_{R\to\infty} \frac{1}{2\pi i} \oint G(z, \xi, \lambda)\, d\lambda = -\delta(z - \xi), \quad \text{(A1)}$$

where G is given by Eq. (3.9). It can be shown that

$$\frac{1}{2\pi i} \oint G\, d\lambda = \frac{1}{2\pi i} \oint \frac{e^{i\sqrt{\lambda}|z-\xi|}}{i\sqrt{\lambda} + 1/(2H)}\, d\lambda \quad \text{(A2)}$$

plus terms of higher order in $1/R$. Put $\lambda = m^2$ of positive m and we get

$$\frac{1}{2\pi i} \oint G\, d\lambda = \frac{1}{2\pi i} \oint \frac{e^{im|z-\xi|}}{im + 1/(2H)} 2m\, dm \quad \text{(A3)}$$

plus terms that go to zero as $R \to \infty$.

Cauchy's theorem is used to deform this circle into a contour around the singularities of G. Note that G has a branch-point singularity at $\lambda = 0$ and a possible pole at $\sqrt{\lambda} = i/2H$. Because of the branch-point singularity, the value of G at A in Fig. A1 is not the same as the value of G at B; consequently, Cauchy's theorem does not apply to the circle ACB since G is not a single-value function on this contour. However, on the curve $ACBDA$ (here, the real axis has been taken as a branch cut), the function G is a single value, and therefore, by Cauchy's theorem

$$\frac{1}{2\pi i} \int_{ACBDA} G\, d\lambda \quad \text{(A4)}$$

equals the sum of the residues of G inside the circle. The only possible singularity of G inside the circle is the point P, where $\sqrt{\lambda} = i/2H$. Since P is located at a negative real axis, it is inside the circle and is a singularity. The residue at P is

$$-\frac{1}{H} e^{-(z+\xi)/2H}[\mathcal{H}(\xi - z) + \mathcal{H}(z - \xi)] = -\frac{1}{H} e^{-(z+\xi)/2H}. \quad \text{(A5)}$$

From (A4) and (A5), one obtains

$$-\frac{1}{H} e^{-(z+\xi)/2H} = \frac{1}{2\pi i} \int_{ACBDA} G\, d\lambda = \frac{1}{2\pi i} \int_{ACB} G\, d\lambda + \frac{1}{2\pi i} \int_{BDA} G\, d\lambda, \quad \text{(A6)}$$

and therefore, the first integral on the right-hand side of Eq. (A6) gives a δ function:

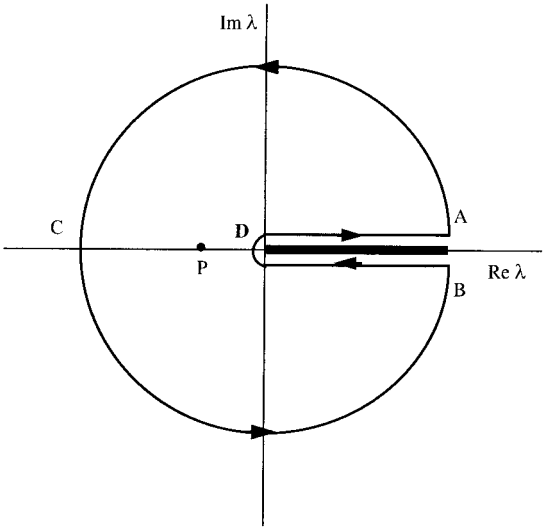

FIG. A1. The contour C in the complex λ domain along which the Green's function should be integrated. Since the Green's function at positive real axis is multivalued, a branch cut is performed. Point P is a pole of the Green's function.

$$-\delta(z - \xi) = \frac{1}{2\pi i} \int_{ACB} G\, d\lambda = -\frac{1}{H} e^{-(z+\xi)/2H} - \frac{1}{2\pi i} \int_{BDA} G\, d\lambda. \quad \text{(A7)}$$

The last integral may be simplified by putting $\lambda = m^2$ of positive m. Note that on the upper-side of the cut, $\sqrt{\lambda} = m$, but on the lower-side of the cut, $\sqrt{\lambda} = -m$. One has

$$\frac{1}{2\pi i} \int_{BDA} G\, d\lambda = -\frac{2}{\pi} \int_0^\infty \left(\cos mz - \frac{1}{2Hm} \sin mz\right) \times \left(\cos m\xi - \frac{1}{2Hm} \sin m\xi\right) \times \frac{m^2}{m^2 + 1/(4H^2)}\, dm. \quad \text{(A8)}$$

From (A7) and (A8), one finally obtains

$$\delta(z - \xi) = \frac{1}{H} e^{-(z+\xi)/2H} + \frac{2}{\pi} \int_0^\infty \left(\cos mz - \frac{1}{2Hm} \sin mz\right) \times \left(\cos m\xi - \frac{1}{2Hm} \sin m\xi\right) \times \frac{m^2}{m^2 + 1/(4H^2)}\, dm. \quad \text{(A9)}$$

REFERENCES

DeMaria, M., 1985: Linear response of a stratified tropical atmosphere to convective forcing. *J. Atmos. Sci.,* **42,** 1944–1959.

Dickinson, R. E., and M. A. Geller, 1968: A generalization of ''tidal theory with Newtonian cooling.'' *J. Atmos. Sci.,* **25,** 932–933.

Eliassen, E., and B. Machenhauer, 1974: On spectral representation of the vertical variation of the meteorological fields in numerical integration of a primitive equation model. GARP WGNE Rep. 7, 83–93.

Frank, W. M., and J. L. McBride, 1989: The vertical distribution of heating in AMEX and GATE cloud clusters. *J. Atmos. Sci.,* **46,** 3464–3478.

Friedman, B., 1956: *Principles and Techniques of Applied Mathematics.* Wiley and Sons, 315 pp.

Geisler, J. E., 1981: A linear model of the Walker circulation. *J. Atmos. Sci.,* **38,** 1390–1400.

——, and D. E. Stevens, 1982: On the vertical structure of damped steady circulation in the tropics. *Quart. J. Roy. Meteor. Soc.,* **108,** 87–94.

Gill, A. E., 1980: Some simple solutions for heat induced tropical circulations. *Quart. J. Roy. Meteor. Soc.,* **106,** 447–462.

——, 1982: *Atmosphere–Ocean Dynamics.* Academic Press, 662 pp.

Hartmann, D. L., H. H. Hendon, and R. A. Houze Jr., 1984: Some implication of mesoscale circulations in tropical cloud clusters for large-scale dynamics and climate. *J. Atmos. Sci.,* **41,** 113–121.

Hendon, H. H., and M. L. Salby, 1996: Planetary-scale circulations forced by intraseasonal variations of observed convection. *J. Atmos. Sci.,* **53,** 1751–1758.

Holl, P., 1970: The completeness of the orthogonal system of the Hough functions. *Nachr. Akad. Wiss. Göttingen II. Math.-Phys. Kl.,* **7,** 159–168.

Holton, J. R., 1975: *The Dynamic Meteorology of the Stratosphere and Mesosphere.* Amer. Meteor. Soc., 218 pp.

——, 1992: *An Introduction to Dynamic Meteorology.* Academic Press, 511 pp.

Horel, J. D., and J. M. Wallace, 1981: Planetary-scale atmospheric phenomena associated with the Southern Oscillation. *Mon. Wea. Rev.,* **109,** 813–829.

Kasahara, A., 1984: The linear response of a stratified global atmosphere to tropical thermal forcing. *J. Atmos. Sci.,* **41,** 2217–2237.

Lau, K.-M., and H. Lim, 1982: Thermally driven motions in an equatorial β-plane: Hadley and Walker circulations during the winter monsoon. *Mon. Wea. Rev.,* **110,** 336–353.

——, and L. Peng, 1987: Origin of low-frequency (intraseasonal) oscillations in the tropical atmosphere. Part I: Basic theory. *J. Atmos. Sci.,* **44,** 950–972.

Lim, H., and C.-P. Chang, 1983: Dynamics of teleconnections and Walker circulations forced by equatorial heating. *J. Atmos. Sci.,* **40,** 1897–1915.

Lindzen, R. S., 1967: Planetary waves on beta-planes. *Mon. Wea. Rev.,* **95,** 441–451.

——, 1968: Vertically propagating waves in an atmosphere with Newtonian cooling inversely proportional to density. *Can. J. Phys.,* **46,** 1835–1840.

——, and T. Matusno, 1968: On the nature of large scale wave disturbances in the equatorial lower stratosphere. *J. Meteor. Soc. Japan,* **46,** 215–220.

——, E. S. Batten, and J.-W. Kim, 1968: Oscillations in atmospheres with tops. *Mon. Wea. Rev.,* **96,** 133–140.

Machenhauer, B., and R. Daley, 1974: Hemispheric spectral model. GARP Publication Series 14, 226–251.

Madden, R. A., and P. R. Julian, 1972: Description of global-scale circulation cells in the tropics with a 40–50 day period. *J. Atmos. Sci.,* **29,** 1109–1123.

Mapes, B. E., and R. A. Houze, 1995: Diabatic divergence profiles in western Pacific mesoscale convective system. *J. Atmos. Sci.,* **52,** 1807–1828.

Matsuno, T., 1966: Quasi-geostrophic motions in the equatorial area. *J. Meteor. Soc. Japan,* **44,** 25–43.

Milliff, R. F., and R. A. Madden, 1996: The existence and vertical structure of fast, eastward-moving disturbances in the equatorial troposphere. *J. Atmos. Sci.,* **53,** 586–597.

Mizzi, A., J. Tribbia, and J. Curry, 1995: Vertical spectral representation in primitive equation models of the atmosphere. *Mon. Wea. Rev.,* **123,** 2426–2446.

Moura, A. D., and J. Shukla, 1981: On the dynamics of droughts in northeast Brazil: Observations, theory, and numerical experiments with a general circulation model. *J. Atmos. Sci.,* **38,** 2653–2675.

Peixoto, J. P., and A. H. Oort, 1992: *Physics of Climate.* American Institute of Physics, 520 pp.

Philander, S. G., 1990: *El Niño, La Niña, and the Southern Oscillation.* Academic Press, 293 pp.

Rodwell, M. J., and B. J. Hoskins, 1996: Monsoons and dynamics of deserts. *Quart. J. Roy. Meteor. Soc.,* **122,** 1385–1404.

Saravanan, R., and J. C. McWilliams, 1995: Multiple equilibria, natural variability, and climate transitions in an idealized ocean–atmosphere model. *J. Climate,* **8,** 2296–2323.

Silva Dias, P. L., 1986: Vertical mode decomposition and model resolation. *Tellus,* **38A,** 205–214.

——, W. H. Schubert, and M. DeMaria, 1983: Large-scale response of the tropical atmosphere to transient convection. *J. Atmos. Sci.,* **40,** 2689–2707.

Simmons, A. J., 1982: The forcing of stationary wave motion by tropical diabatic heating. *Quart. J. Roy. Meteor. Soc.,* **108,** 503–534.

Sui, C.-H., and K.-M. Lau, 1989: Origin of low-frequency (intraseasonal) oscillations in the tropical atmosphere. Part. II: Structure and propagation of mobile wave-CISK modes and their modification by lower boundary forcings. *J. Atmos. Sci.,* **46,** 38–56.

Wang, T.-A., Y.-L. Yin, H. F. M. Semazzi, and G. S. Jamowitz, 1996: Response of a stably stratified atmosphere to large-scale diabatic forcing with applications to wind patters in Brazil and Sahel. *J. Geophys. Res.,* **101**(D3), 7049–7073.

Webster, P. J., 1972: Response of the tropical atmosphere to local steady forcing. *Mon. Wea. Rev.,* **100,** 518–541.

Wu, Z., 1998: The thermally driven surface winds in the tropics. Ph.D. dissertation, Department of Atmospheric Sciences, University of Washington, Seattle, WA, 178 pp. [Available from Dept. of Atmospheric Sciences, University of Washington, Seattle, WA 98195.].

——, E. S. Sarachik, D. S. Battisti, 1999: Thermally driven surface winds on an equatorial beta-plane. *J. Atmos. Sci.,* **56,** 2029–2037.

——, D. S. Battisti, and E. S. Sarachik, 2000: Rayleigh friction, Newtonian cooling, and the linear response to steady tropical heating. *J. Atmos. Sci.,* **57,** 1937–1957.

Zhang, Z., and T. N. Krishnamurti, 1996: A generalization of Gill's heat-induced tropical circulation. *J. Atmos. Sci.,* **53,** 1045–1052.